Nongray Soot and Gas-Phase Radiation Modeling in Luminous Turbulent Nonpremixed Jet Flames

L. Wang, M.F. Modest, D.C. Haworth, and S.R. Turns

The Pennsylvania State University, Department of Mechanical and Nuclear Engineering, University Park, PA 16802 USA

Abstract

Much progress has been made in radiative heat transfer modeling with respect to treatment of nongray radiation from both gas species and soot particles, while radiation modeling in turbulent flame simulations is still in its infancy. Aiming at reducing this gap, this paper introduces sophisticated models of soot and gas-phase radiation to turbulent flame simulations. The full-spectrum k-distribution method is implemented into a three-dimensional unstructured CFD code for nongray radiation modeling. The mixture full-spectrum k-distributions including nongray absorbing soot particles are constructed from a narrow-band k-distribution database created for individual gas-phase species, and an efficient scheme is employed for the construction in complex CFD simulations. A detailed reaction mechanism including NO_x and soot kinetics is used to predict flame structure. A detailed soot model with method of moments is employed to determine soot particle size distributions. An oxygen-enriched, turbulent, nonpremixed jet flame is simulated, which features large concentrations of gas-phase radiating species and soot particles. Nongray soot modeling is shown to be of greater importance than nongray gas modeling in sooty flame simulations, with gray soot models producing large errors. The nongray treatment of soot strongly influences flame temperatures in the upstream and the flame tip region and is essential for accurate predictions of NO formation in sooty flames. The nongray treatment of gases, however, weakly influences upstream flame temperatures and, therefore, has only a small effect on NO_x predictions. The effect of nongray soot radiation on flame temperature is also substantial in downstream regions where the soot concentration is small.

Key words: Turbulent Nonpremixed Flames, Nongray Gas Radiation, Nongray Soot Radiation, Full-Spectrum k-Distribution, Spherical Harmonic P_1 Method

1 Introduction

Thermal radiation plays an important role in combustion and flames. Inadequate treatment of radiation can cause large errors in determining the flame structure and pollutant emissions. For example, the prediction of NO_x emission is very sensitive to the prediction of the flame temperature distribution[1]. Similarly, soot formation/oxidation and radiation are highly coupled processes. Errors in temperature predictions result in over- or under-predicted soot formation and oxidation rates and, therefore, soot yields, which in turn result in erroneous radiative heat loss values. Consequently,

a detailed description of radiative energy transfer is an essential element in turbulent combustion simulations.

Radiative heat transfer in turbulent flames enters the overall energy conservation equation through a heat source term, which is expressed as the divergence of the radiative heat flux, $\vec{q}_R$,

$$\nabla \cdot \vec{q}_R = \int_0^\infty \kappa_\eta \left(4\pi I_{b\eta} - \int_{4\pi} I_\eta \mathrm{d}\Omega \right) \mathrm{d}\eta = \int_0^\infty \kappa_\eta \left(4\pi I_{b\eta} - G_\eta \right) \mathrm{d}\eta \tag{1}$$

where η is wavenumber, Ω is solid angle, κ_η is the spectral absorption coefficient, I_η is the spectral radiative intensity, and G_η the spectral incident radiation; subscript b denotes a blackbody property[2]. The absorption coefficient may contain contributions from both gas-phase species and particulates. The radiative intensity is determined from the solution of the radiative transfer equation (RTE).

Accurate evaluation of radiative heat transfer in turbulent flames is extremely difficult due to three challenges: the solution of the RTE (a five-dimensional integro-differential equation), the spectral behavior of the radiating species and the spectral integration of Eq. (1), and the evaluation of turbulence-radiation interactions. Turbulence-radiation interactions are beyond the scope of the present paper, and the reader is referred to the pertinent literature[3−9].

Because of the difficulties associated with radiation calculations, it has been the common practice for radiation calculations in turbulent flames to use the optically-thin approximation, and/or to assume the medium to be gray, for both luminous[10−12] and nonluminous (see TNF workshop[13]) flames. The optically-thin radiation model can result in substantial error due to its neglect of self-absorption effects, as has been shown by both numerical and experimental studies[1, 14]. The gray medium assumption can also result in large errors as will be shown in the following. Nongray radiation modeling has begun to draw attention in combustion simulations[8, 15, 16], and spectral radiation measurements have been conducted recently to provide experimental guidance[9, 17, 18].

Soot radiation constitutes an important part of the total flame radiation in luminous flames. The determination of soot radiation in a realistic radiation model involves determination of soot particle size distributions in flames, as well as modeling of radiative properties of individual soot particles. Because of the difficulties in soot modeling, soot quantities determined in flame simulations usually are limited to soot total number density and soot mass or volume fraction[19]. Because of the complex structure of soot particles and the uncertainties in soot refraction index, soot radiation in turbulent flames has been treated commonly using the optically-thin approximation with the assumption of gray soot.

Popular methods for the solution of the RTE in turbulent combustion simulations include the spherical harmonics P_1 method[7], the discrete ordinates (S_N) method[8], and the discrete transfer method[20]. Among these methods, the P_1 method is the simplest one, yet it is powerful and accurate in most combustion applications. Its applicability to turbulent jet flames is discussed in this paper. Popular models for nongray radiative properties include the weighted sum of gray gases (WSGG) model[16], the spectral line-based weighted sum of gray gases (SLW) model[8], and the full spectrum k-distribution (FSK) method[15]. It has been shown that the FSK method is superior to the WSGG model and the SLW model is only a crude implementation of the FSK method[21]. Recent developments of the FSK method in-

clude constructing mixture full-spectrum k-distributions from a narrow-band k-distribution database created for individual gas species[22]. This development makes is possible to account for nongray soot radiative properties.

The purpose of this paper is to apply the recent developments of the FSK method to turbulent flame simulations for nongray soot and gas-phase radiation modeling. Three radiation models are implemented into a three-dimensional unstructured CFD code: one that accounts for nongray properties of both gas species and soot particles, one that considers nongray gases but gray soot, and one that assumes both gases and soot to be gray. The FSK method is employed for nongray radiation modeling and Planck-mean absorption coefficients are used for gray medium properties. All the radiation models include self-absorption and employ the spherical harmonic P_1 method for the RTE solution. A detailed reaction mechanism containing 122 chemical species and 677 elementary reaction is employed to model gas-phase chemistry. A detailed soot model with the method of moments is employed to determine the soot particle size distribution function (PSDF), which is then used to calculate soot radiation. The effects of nongray soot and gas-phase radiation on flame temperature distribution and NO_x emissions are discussed for an oxygen-enriched, turbulent, nonpremixed jet flame.

2 Modeling Target

The modeled flame is a turbulent nonpremixed propane jet flame with fuel issuing from a 3-mm-i.d. nozzle at a velocity of 21.8 m/s (the jet Reynolds number is approximately 15,000)[23]. The oxygen-enriched laminar coflow of 200-mm i.d. contains 40% oxygen by volume. It has been shown by a simple two-stage Lagrangian modeling study[23] that the 40% oxygen enrichment results in the largest soot concentrations, which, in turn, make a large contribution to the total radiative heat loss. Oxygen-enriched flames feature higher flame temperature and higher concentration of H_2O and CO_2 compared to hydrocarbon-air flames, since the heat sink and diluent effects of nitrogen diminish[24]. In addition, the increased temperature promotes soot formation. These characteristics make both nongray gas-phase and soot radiation important. Measurements available for comparisons include global quantities such as NO_x emission index ($EINO_x$)[25] and radiant fraction (ratio of the total radiative heat loss to the chemical heat release), and axial profiles of radiant heat flux at the peripheral side of the flame[23].

3 Numerical and Physical Models

3.1 Turbulent Flow Field

The underlying CFD code[26] solves the Favre-averaged compressible flow equations using a finite-volume method on an unstructured mesh. The equations include conservation of mass, momentum, absolute enthalpy, and chemical species. Gradient-transport models are invoked for turbulent transport and a standard k-ε model is employed. An iteratively implicit, pressure-based, segregated solu-

tion procedure solves the coupled system of governing pde's for collocated cell-centered variables. Here the computational configuration is axisymmetric and steady-state solutions are reached by time marching.

3.2 Chemistry Calculations

Detailed chemical mechanisms are required to describe soot formation/oxidation and NO_x production. The mechanism used here integrates the mechanism taken from Appel et al.[27] for soot precursor (polycyclic aromatic hydrocarbon, PAH) growth and oxidation with the mechanisms taken from GRI_Mech 3.0[28] for NO_x formation and propane oxidation. The resulting mechanism contains 122 chemical species and 677 elementary reactions[29], and is implemented using CHEMKIN[30]. The same mechanism was used in an earlier two-stage Lagrangian modeling study for oxygen-enriched flames[23]. In the present CFD-based modeling study, *in situ* adaptive tabulation[31] has been used to accelerate the chemistry calculations. Turbulence-chemistry interactions are an important aspect of turbulent combustion modeling. A variant of an eddy-breakup model, a characteristic-time-scale model[32], has been employed to account for the effects of turbulence on mean chemical reaction rates.

3.3 Soot Calculations

The soot model employed represents detailed descriptions of the formation and oxidation of PAH's, the nucleation of the first soot particles, coagulation, surface growth and condensation, and oxidation of soot particles[27, 33]. The gas-phase chemistry for PAH's includes species up to four-ring aromatics (pyrene). The occurrence of the smallest soot particles results from the coagulation of two PAH's. These particles grow through surface reactions and condensation of PAH molecules. They can also be removed by oxidation as a result of soot surface reactions with molecular oxygen and OH radicals.

The evolution of the soot PSDF due to soot nucleation, coagulation, surface growth, and oxidation, is described by the method of moments[34]. The rth soot moment of the PSDF, M_r, is defined as

$$M_r = \sum_{i=1}^{\infty} m_i^r N_i \quad \text{for } r = 0, 1, \ldots, \infty, \tag{2}$$

where m_i and N_i are the particle mass and number density of size class i, respectively. Then, the zeroth moment is the total number density of soot particles, the first moment is the total mass density, and so on. In principle, the knowledge of all the moments is equivalent to the knowledge of the PSDF itself. In most practical applications, however, the properties of interest are fully determined by just the first few moments[34]: for example, soot volume fraction can be deduced from the first moment. This results in the numerical economy of the method of moments.

Transport equations of soot moments have been derived[19] and the mean moment transport equations

solved in the CFD code are written as:

$$\frac{\partial(\bar{\rho}\tilde{M}_{mr})}{\partial t} + \frac{\partial(\bar{\rho}\tilde{u}_i\tilde{M}_{mr})}{\partial x_i} = \frac{\partial}{\partial x_i}\left(\frac{\mu_T}{Pr_{T,s}}\frac{\partial \tilde{M}_{mr}}{\partial x_i}\right) + \overline{\left.\frac{\mathrm{d}M_r}{\mathrm{d}t}\right|_s}, \quad \text{for } r = 0, 1, \ldots, 5, \tag{3}$$

where the over-bar and tilde denote Reynolds- and Favre-averaged mean quantities, respectively. Here $M_{mr} = M_r/\rho$, where ρ is the density of the gas-phase mixture. Then $\bar{M}_r$ and $\tilde{M}_{mr}$ are related by $\bar{M}_r = \bar{\rho}\tilde{M}_{mr}$. The molecular diffusion term has been neglected and a gradient-transport model has been invoked for turbulent transport. The quantity μ_T is the effective turbulence viscosity determined by the k-ε turbulence model ($\mu_T = C_\mu \bar{\rho} k^2/\varepsilon$), and $Pr_{T,s}$ is an effective turbulent Schmidt number and is set to unity in our calculations. The mean source terms in Eq. (3) are evaluated using the mean quantities calculated from the CFD code, i.e., neglecting the influence of turbulent fluctuations.

There are discrepancies between the predicted and measured soot distribution as reported in the study of Wang et al.[19]. In order to capture a correct contribution from soot radiation, the soot distribution used for the radiation calculations is obtained as follows. Transport equations for soot moments are solved and the distribution of soot volume fraction (f_v, used in determining soot radiation) is obtained. The calculated distribution of f_v(z,r) then is adjusted to provide the same f_v axial profile as obtained from experiments. Finally, this adjusted f_v distribution is imposed on the same computational grid with the soot moments calculations turned off.

3.4 Radiation Models

To date the FSK method provides the most accurate and effective means for the spectral integration of the RTE[21]. For homogeneous media, it achieves the accuracy of line-by-line (LBL) calculations but at a tiny fraction of LBL's computational cost. For inhomogeneous media, the assumption of correlated absorption coefficients is usually invoked and the application of it leads to two versions of the FSK method, the full-spectrum correlated-k (FSCK) method and the full-spectrum scaled-k (FSSK) method[35]. The error introduced by the correlated absorption coefficients assumption can be further remedied by a multi-group approach[36], but this approach is still under development. The FSSK method has been employed in this paper since it often outperforms the FSCK method[35].

Employing FSSK, the radiative heat source term (Eq. 1) becomes[35]

$$\nabla \cdot \vec{q}_R = \int_0^1 ku(4\pi a I_b - G_g)\mathrm{d}g, \tag{4}$$

where k is the reordered local mixture absorption coefficient (κ_η) evaluated at a reference state, which is a function of a normalized spectral variable weighted by the Planck function, g, and u is a scaling function that incorporates the spatial variations of the absorption coefficient. The parameter a is a nongray stretching factor accounting for varying local temperatures in the Planck function that is used to construct the k-g distributions[21,35], and G_g is the spectral incident radiation in g-space. The spectral incident radiation can be obtained by solving the FSK-reordered RTE[21,35] with the P_1 approximation,

$$\nabla \cdot \frac{1}{ku}\nabla G_g - 3ku\left(G_g - 4\pi a I_b\right) = 0, \tag{5}$$

and the boundary condition

$$-\frac{2(2-\epsilon)}{3\epsilon}\hat{n}\cdot\nabla G_g + kuG_g = 4\pi kua_w I_{bw}, \tag{6}$$

where $\hat{n}$ is the inward-pointing unit surface normal at a boundary, ϵ is the surface emittance, and a_w and I_{bw} are evaluated at the surface temperature T_w. The incident radiation is evaluated at representative "spectral" g locations, whose values are usually determined by a Gaussian quadrature scheme. Ten or fewer quadrature points generally suffice because of the smooth behavior of k in g-space. Here nine quadrature points have been used, thus requiring the solution to nine equations of the form of Eqs. (5) and (6).

During a CFD simulation of a flame, it is impractical to calculate the local mixture k-distributions directly from a spectral line database, since it is CPU time demanding and radiation calculations constitute only a small part of a turbulent flame simulation. In practice, the k-distributions of each component species are precalculated and, during the flame simulation, the local mixture k-distributions are obtained by mixing the precalculated single-gas k-distributions (SGK's) according to the local mixture composition. The SGK's can be constructed in two formats, viz., full-spectrum and narrow-band k-distributions. In the full-spectrum format, the mixing is performed at the full-spectrum level, but this excludes consideration of nongray soot particles; soot must then be treated as gray and its spectrally averaged mean property is added directly to full-spectrum k-distributions of the gas mixture. In the narrow-band format, the mixing is performed at the narrow-band level and that allows consideration of nongray soot particles; the absorption due to nongray soot can be added directly to the narrow-band k-distributions of the gas mixture, since the soot absorption coefficient is essentially constant across each narrow band[22]. Both formats of precalculated SGK's have been implemented in our calculations, leading to two different radiation models: one fully nongray model with both gases and soot treated as nongray, and a semigray model where gases are treated as nongray while soot is assumed to be gray.

The mixing model used to calculate mixture k-distributions from SGK's is the one proposed by Riazzi and Modest[22]. This model is based on the uncorrelatedness between spectral lines of different gases, leading to multiplicative transmittance from which a rule of mixing SGK's was derived. This mixing model has been shown to be more accurate than all other currently existing models[22]. Mixing at the narrow-band level is fairly demanding computationally. For example, the computation of the mixture k-distributions for a moderate sized CFD mesh of 5000 computational cells consumes about 35 seconds on a 2.8 GHz Intel Xeon processor for just one time/iteration step. Mixing at the full spectrum level, on the other hand, is much faster by almost a factor of the number of the narrow bands (about 250 for a sufficiently accurate narrow-band database[37]). To achieve better efficiency, the computational domain is divided into two regions according to a threshold value of soot volume fraction: a soot–gas region and a gas-only region. For the gas-only region, both the fully nongray radiation model and the semigray model use precalculated full-spectrum SGK's to obtain the local mixture k-distributions. For the soot–gas region, the semigray model also uses full-spectrum SGK's for mixing (since soot is treated as gray), while the nongray model uses narrow-band SGK's to obtain local mixture k-distributions (since nongray soot is taken into account). The error introduced by mixing at the full-spectrum level was found to be less than 2% compared to mixing at the narrow-band level[22]. The threshold value of soot volume fraction is determined such that the optical thickness

of the computational domain for that value is less than 0.01 at the wavelength where the averaged blackbody intensity in the domain takes the maximum value.

If one neglects the weak dependence of spectral line broadening on species mole fractions, then the absorption coefficients are linearly dependent on species mole fractions. Using this approximation, mixture narrow-band k-distributions (MNBK's) can be precalculated for the soot–gas region and the expensive mixing process can then be avoided during a CFD simulation, as long as the mole fraction ratio of the component species in the mixture is fixed. This is the case for complete combustion of a hydrocarbon fuel, where the mole fraction ratio of radiatively participating species is fixed at the stoichiometric value (for example, the H_2O/CO_2 ratio for propane flames is always 0.75). In real flames, incomplete combustion and turbulent mixing can shift the ratios from their stoichiometric values. To deal with this, several MNBK's with different mole fraction ratios are precalculated, and interpolation/extrapolation can be performed for mixtures of arbitrary species mole fraction ratios.

In our calculations, only CO_2 and H_2O are considered as radiatively participating, and the contributions from CO and propane are ignored since their contributions are relatively small. It has been observed that the range of mole fraction ratios of CO_2 to H_2O for the soot–gas region (on the fuel-rich side of the flame) is between the stoichiometric value (0.75) and 0.2. Therefore, MNBK's of 4 ratios (0.8, 0.6, 0.4, and 0.2) are databased. The H_2O mole fraction used for generating these MNBK's is the value in the stoichiometric combustion of propane with 40% O_2 and 60% N_2 (0.27). The full-spectrum SGK's and MNBK's in this work are precalculated from the high-accuracy narrow-band SGK database generated by Wang and Modest[37]. In Fig. 1, the mixture full-spectrum k-distributions constructed from the precalculated full-spectrum SGK's and MNBK's (for the gas-only and soot–gas region, respectively) are compared with those constructed directly from the high-accuracy narrow-band SGK database. The mixture contains 5.5% CO_2 and 10% H_2O with a soot volume fraction of 7.5×10^{-07}. The figure shows that the differences are small and, therefore, the construction scheme of using precalculated full-spectrum SGK's and MNBK's is acceptable for CFD simulations. Differences between the mixture full-spectrum k-distributions with and without soot (soot–gas region and gas-only region in the figure) indicate the contribution of the soot to the mixture absorption coefficient.

The nongray soot absorption coefficient is determined by applying Rayleigh's theory to an ensemble of polydisperse soot particles, which gives[2]

$$\kappa_\lambda = \frac{36\pi nk}{(n^2-k^2+2)^2+4n^2k^2}\frac{f_v}{\lambda}, \tag{7}$$

where λ is wavelength in cm. The soot complex index of refraction, $m = n - ik$, is modeled using the correlations proposed by Chang and Charalampopoulos[38]:

$$n = 1.8110 + 0.1263\ln\lambda + 0.0270\ln^2\lambda + 0.0417\ln^3\lambda, \tag{8}$$

$$k = 0.5821 + 0.1213\ln\lambda + 0.2309\ln^2\lambda - 0.0100\ln^3\lambda. \tag{9}$$

Here λ is in μm and these correlations are valid over the wavelength range $0.4\mu\text{m} \leq \lambda \leq 30\mu\text{m}$.

To demonstrate the importance of using a nongray radiation model, a gray model is also implemented.

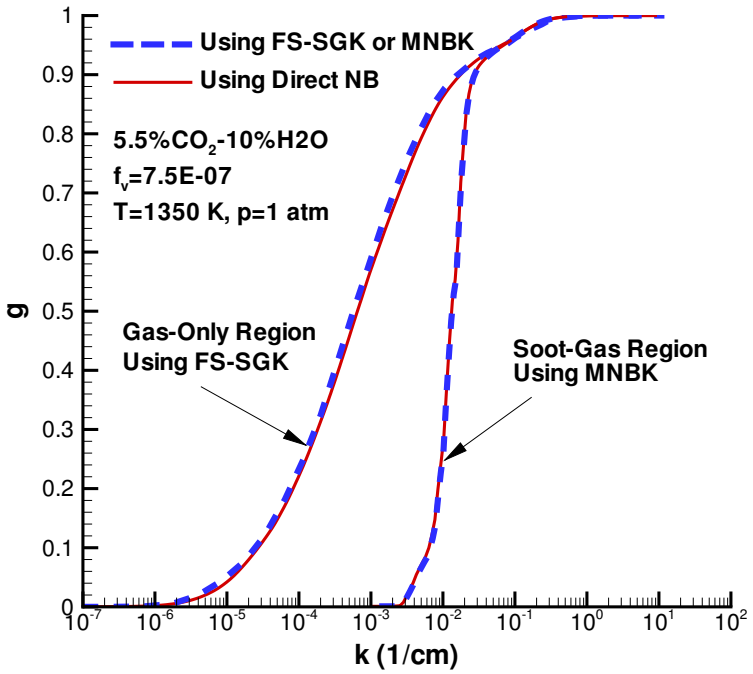

Fig. 1. Full-spectrum k vs. g distribution for gas-only and soot–gas region

The radiative source term (Eq. 1) for a gray medium becomes[35]:

$$\nabla \cdot \vec{q}_R = 4\pi\kappa_p I_b - \kappa_p G, \tag{10}$$

where κ_p is the Planck-mean absorption coefficient. Gas-phase Planck-mean absorption coefficients are determined from local gas-phase full-spectrum k-distributions, and soot Planck-mean absorption coefficients are determined from spectrally averaging Eq. (7) at local conditions. The incident radiation G is determined by solving the RTE with the spherical harmonic P_1 method[2].

4 Results and Discussion

Figure 2 shows contour plots of the divergence of radiative heat flux (the heat source term in the energy conservation equation) predicted by the three radiation models for the oxygen-enriched propane flame. The contours are plotted on a slice of the axisymmetric computational mesh, where the radial coordinate has been stretched for clarity. For convenience, isocontours of the soot volume fraction also are plotted. Since the radiative heat source is strongly dependent on flame temperature, its isocontours essentially indicate the location of the flame zone, where chemical reactions are most active. This figure shows that, overall, the gray model (gray soot and gray gases) predicts larger heat losses than the semigray model (gray soot and nongray gases), which in turn predicts larger heat losses than the fully nongray model (nongray soot and nongray gases). The reason for the errors introduced by gray models is that the Planck-mean absorption coefficient is designed to predict the correct overall

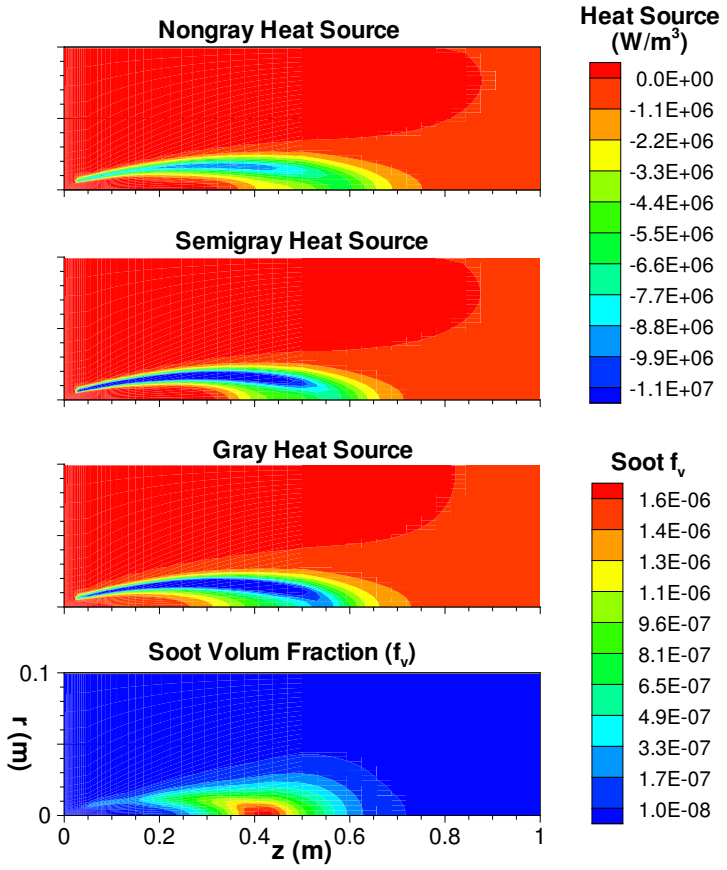

Fig. 2. Contours of the computed divergence of radiative heat flux (heat source) and the soot volume fraction

emission and it fails to account for the self-absorption properly, which is always underpredicted[2]. The difference in heat source prediction is more substantial between the nongray and the semigray model than between the semigray and the gray model, as can be seen by comparing the three contours in the flame tip region (z between 0.35 and 0.6 m) and the upstream flame zone (z less than 0.2 m). This suggests that the nongray soot treatment is more important than the nongray gases treatment in this sooty flame. The maximum value of soot volume fraction f_v is approximately 1.7×10^{-06}.

Figure 3 shows contour plots of the flame temperatures predicted by the three radiation models. The temperature contours are generally consistent with the heat source contours. For example, in the flame tip region the nongray model predicts higher flame temperatures than the semigray model, which in turn predicts higher flame temperatures than the gray model. The temperature contours also show that the difference in temperature prediction between the nongray and the semigray model is more substantial than between the semigray and the gray model. It is interesting to note that the flame zone (as indicated by high temperature) predicted by the nongray model, in addition to becoming broader in the flame tip region, extends further downstream than does the flame zone predicted by the semigray and gray models. This suggests that the nongray radiation treatment, with its smaller heat loss, results in a longer flame length than the gray radiation treatment.

The comparison of heat source and temperature contours gives a visual impression of the differences between the gray and nongray radiation models. To quantify these differences, axial and radial pro-

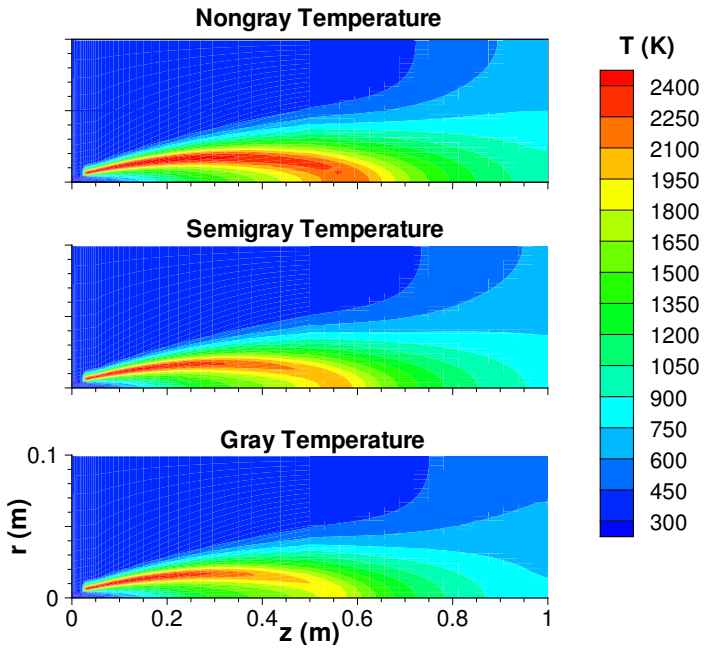

Fig. 3. Contours of the computed flame temperature

files of temperature and species mass fraction are also examined. Figure 4 shows the axial profiles of centerline flame temperatures predicted by the three radiation models. It can be seen clearly that the gray treatment of the radiatively participating medium overpredicts radiative heat loss and, therefore, underpredicts flame temperature. The difference in maximum axial flame temperature due to gray/nongray treatment of gases (the gray and semigray model), due to gray/nongray treatment of soot (the semigray and nongray model), and due to gray/nongray treatment of both gases and soot (the gray and nongray model) is approximately 149K, 221K, and 370K, respectively. The difference in temperature due to gray/nongray soot is approximately 1.5 times larger than the difference due to gray/nongray gases. This demonstrates the importance of nongray soot radiation modeling in sooty flame simulations. In addition, the nongrayness of the soot and gases causes the flame zone to lengthen by about 5%, with the maximum temperature occurring approximately 0.03 m further downstream.

Figure 5 shows the radial profiles of flame temperatures predicted by the three radiation models at three axial locations: one upstream, one in the flame tip region, and one downstream, demonstrating the effects of gray and nongray treatments at different axial locations. The differences between the semigray and the gray model (effects of nongray/gray gas modeling) again are relatively small compared to the differences between the nongray and the semigray model (effects of nongray/gray soot modeling). The nongray treatment of gases and soot leads to higher flame temperature throughout the computational domain. Nongray soot modeling shows a maximum effect near the flame tip region as seen in the profile at $z = 0.5$ m. This is consistent with the distribution of soot volume fraction shown in Fig. 2. In the downstream region where there is little soot, the nongray soot model also has a large effect on the flame temperature distribution, as shown by the profile at $z = 0.8$ m, because hotter upstream gases are convected downstream. Table 1 tabulates the temperature differences between different radiation models at the three axial locations. In this table, the quantity ΔT_1 is the maximum

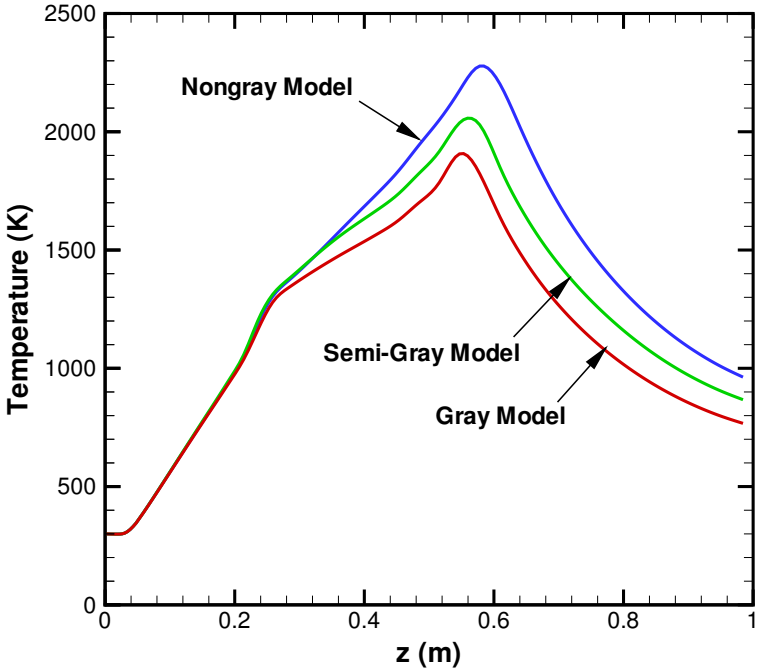

Fig. 4. Axial profiles of centerline flame temperature

Table 1
Maximum flame temperature differences due to radiation models

Axial Location	ΔT_1	ΔT_2	ΔT_3
$z = 0.2$ m	≈ 0	132	132
$z = 0.5$ m	146	262	408
$z = 0.8$ m	142	165	307

temperature difference between predictions by the semigray and the gray model, ΔT_2 between the semigray and the nongray model, and ΔT_3 between the gray and the nongray model. In the upstream region, the temperature differences due to gray/nongray gas radiation model are essentially negligible. In the flame tip region, the maximum temperature difference between nongray and gray soot models is approximately 1.8 times larger than that between nongray and gray gases models, while in the downstream region, the factor is approximately 1.2. This stronger effect on flame temperature in the upstream and flame tip region has an impact on NO prediction, which is formed largely in those regions, as shown in the following.

Figure 6 shows radial profiles of calculated NO mass fractions resulting from the three radiation models at two axial locations. For clarity, the profiles at $z = 0.8$ m are not shown since they follow the same trends as shown by the profiles at $z = 0.5$ m. The profiles at $z = 0.2$ m show that a large portion of the NO emission is generated in the upstream flame zone, and that the NO formation is extremely sensitive to flame temperature (see Fig. 5 for temperature differences), and, therefore, the radiation model. The profiles at $z = 0.5$ m also indicate that the differences in NO mass fraction

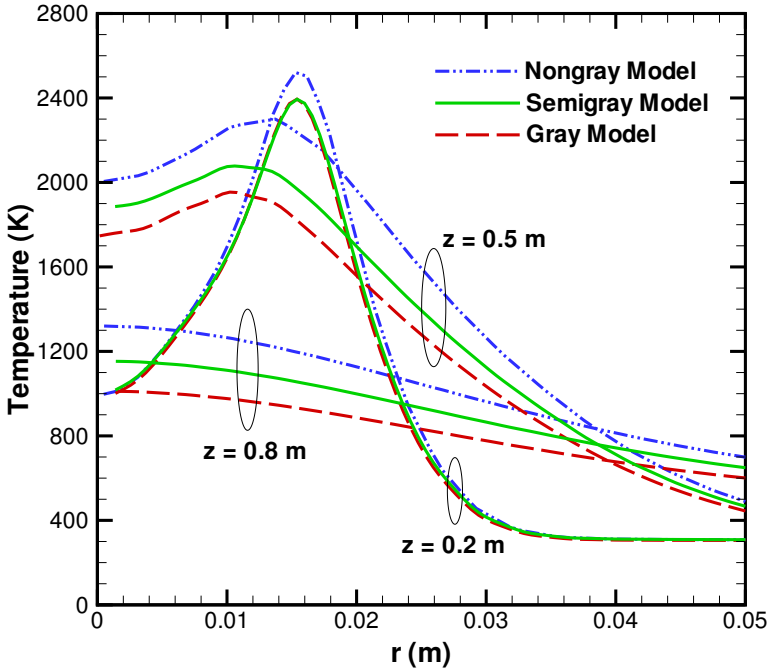

Fig. 5. Radial profiles of flame temperature at three axial locations

due to nongray gases modeling are much smaller than the differences due to nongray soot modeling. The nongrayness of soot was shown in Fig. 5 to have the strongest impact on flame temperature, especially in the upstream flame zone and the flame tip region, therefore, nongray soot modeling is shown to be an essential element for accurate prediction of NO_x emissions in sooty flames.

The importance of nongray soot modeling can be further appreciated in Table 2, where the predicted NO_x emission indices and the radiant fractions from the three radiation models are compared with measured values. Both NO_x emission index and radiant fraction are indications of the overall flame temperature level, and the comparison between model predictions and measurements determines the overall performance of a radiation model. Table 2 shows that the gray and the semigray model overpredict the radiant fraction and, therefore, underpredict NO_x emissions; the nongray radiation model provides predictions that are the closest to the experimental values. The nongray model's overprediction of radiative loss likely comes from the turbulent combustion model, which leads to fast combustion and, therefore, overpredicted upstream flame temperatures[29]. The table also shows that the differences in radiant fraction among the three models are the same (0.08), while the difference in the NO_x emission index between the gray and the semigray model is much smaller than that between the nongray and the semigray model (0.9 vs. 14). This can be explained by the fact that a large portion of the NO is formed in the upstream flame zone, and by the differences in upstream wall heat fluxes among the three models as shown in Fig. 7.

Figure 7 shows the axial profiles of radiant heat fluxes (at $r = 0.1$ m, Fig. 2) predicted by the three radiation models. The curve with symbols is obtained from the experiment. The gray model greatly overpredicts the heat fluxes as expected. The semigray model provides a peak value that is close

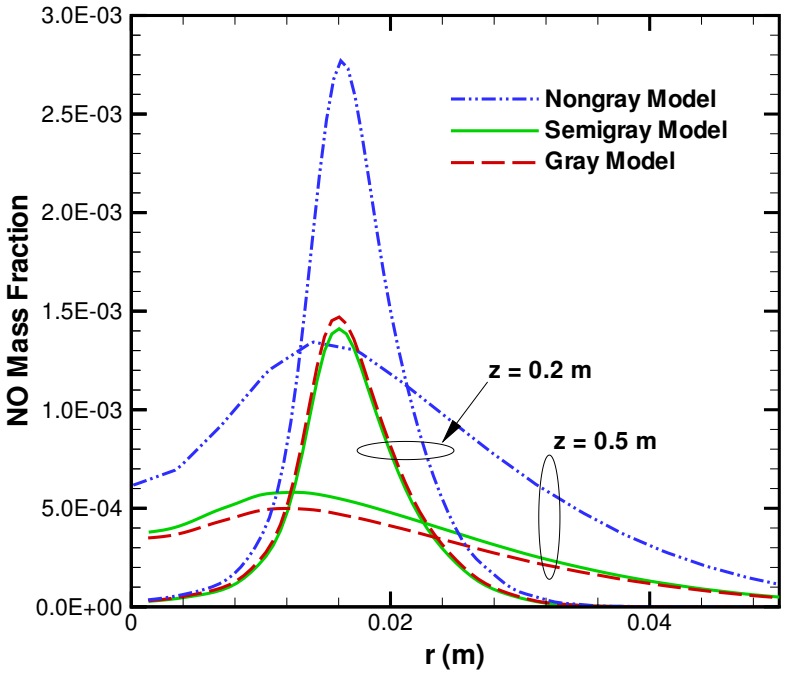

Fig. 6. Radial profiles of NO species mass fraction at three axial locations

Table 2
Comparison of global quantities with experiment

Model	NO_x Emission Index	Radiant Fraction
Gray Model	10.2	0.51
Semi-Gray Model	11.1	0.43
Nongray Model	25.1	0.35
Experiment	29.8	0.31

to the experiment, but overall it also overpredicts the heat fluxes. Although the peak heat flux is underpredicted, the nongray model gives the best agreement in terms of the location of the peak value, and the overall radiation heat loss (proportional to the area under the profile). All the models show a flatter, less peaked distribution than experiment. This is found to be mainly caused by the use of the P_1 approximation, as shown in the following analysis.

To identify the errors introduced by the P_1 approximation in our simulations, two calculations are conducted. First, the CFD code is set up such that a small cylindrical hot zone of high constant temperature (2200 K) and large constant Planck-mean absorption coefficient (5000 1/m) exists in the middle of the cylindrical computational mesh (shown in Fig. 2) to simulate the near-opaque soot region; the temperature and the Planck-mean absorption coefficient for the rest of the computational mesh are set to 300 K and a small constant value of κ_{rest}, respectively; the boundary is black and cold at 300 K. The radiant heat flux at the wall ($r = 0.1$ m) is then calculated using the P_1-gray

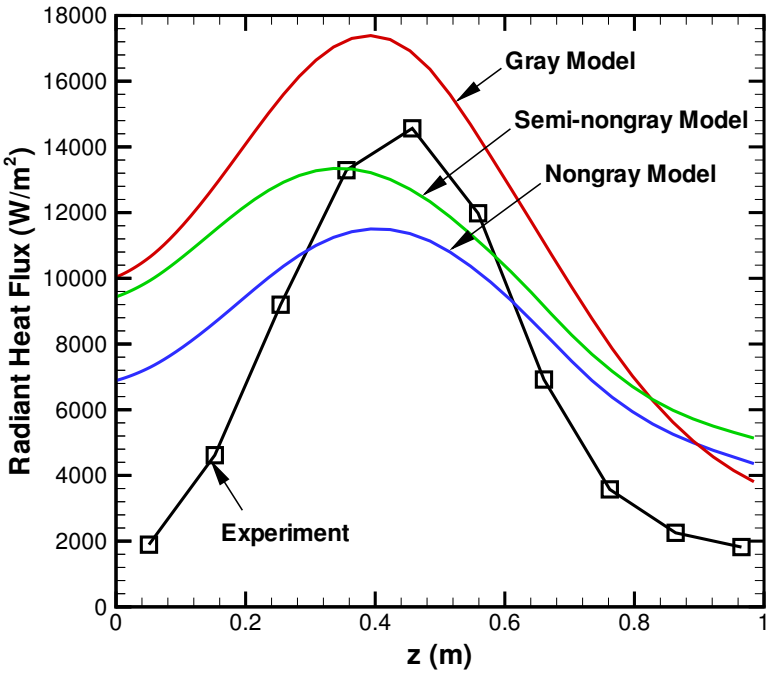

Fig. 7. Axial profiles of calculated and measured radiant heat flux at $r = 0.1$ m

model in the code. Second, the exterior of the small hot cylinder and the interior of the large cold cylinder ($r = 0.1$ m) are taken as black surfaces, and the radiant heat flux at $r = 0.1$ m is determined using view factors between the two black surfaces. Both calculations should coincide in the limit of $\kappa_{rest} = 0$ if the P_1 method gave exact solutions to the RTE. Discrepancies, therefore, show the inaccuracies of the P_1 method.

Figure 8 shows the axial profiles of the radiant heat flux at $r = 0.1$ m from the two calculations. The three numerical values attached to the P_1-gray curves, 0.1, 0.3, and 1.0, are different values of κ_{rest}. As the value of κ_{rest} decreases, or as the ratio of the absorption coefficient of the hot zone to the rest the domain increases, the performance of the P_1 approximation becomes progressively worse. This analysis shows that the P_1 method is, in general, not suitable for quantitative radiation modeling in flames with near-opaque, localized soot regions, resulting in very anisotropic radiative intensity fields. However, the qualititative trends will not be affected, as evidenced by the global quantity comparisons in Table 2 and the nongray model's good agreement with experiment in the overall radiative heat loss shown in Fig. 7.

5 Conclusions

In this paper, the use of the narrow-band-based FSK method for nongray soot and gas radiation modeling in the CFD simulation of turbulent flames is described, and the importance of nongray radiation modeling in predictions of flame temperature and NO_x emissions is discussed. The scheme

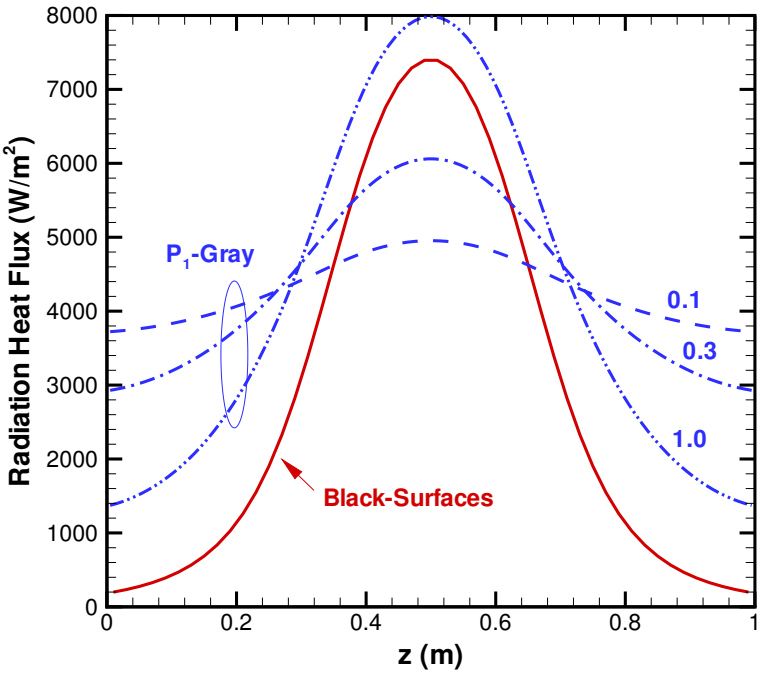

Fig. 8. Axial profiles of calculated radiant heat flux: study of P_1 approximation

of constructing local full-spectrum k-distributions from precalculated full-spectrum single-gas k-distributions and mixture narrow-band k-distributions is shown to be acceptable for CFD simulations. The simulation of an oxygen-enriched turbulent nonpremixed jet flame shows that gray models always overpredict radiative heat loss and underpredict flame temperature and NO_x emissions as expected. Nongray soot modeling is shown to be of greater importance than nongray gas modeling in sooty flame simulations, with gray soot models producing large errors. The nongray treatment of soot strongly influences flame temperatures in the upstream and the flame tip region and is essential for accurate predictions of NO formation in sooty flames. The nongray treatment of gases, however, weakly influences upstream flame temperatures and, therefore, has only a small effect on NO_x predictions. The nongrayness of soot also has a large effect on flame temperatures in downstream regions where the soot concentration is small. The spherical harmonic P_1 method is found to be not suitable for quantitative radiation modeling in flames with localized, near-opaque soot regions.

Acknowledgements

This research has been sponsored by National Science Foundation under Grant Number CTS-0121573, and by the GM R&D center.

References

1. Frank, J. H., Barlow, R. S., and Lundquist, C., Radiation and nitric oxide formation in turbulent non-premixed jet flames, Proc. Combust. Institute 2000, 28: 447–454.
2. Modest, M. F., *Radiative Heat Transfer*, Academic Press, New York 2nd edn. 2003.
3. Song, T. H. and Viskanta, R., Interactions of radiation with turbulence: application to a combustion system, J. Thermophys. Heat Trans. 1987, 1(1): 56–62.
4. Gore, J. P., S., I. U., and Sivathanu, Y. R., Coupled structure and radiation analysis of acetylene/air flames, ASME J. Heat Trans. 1992, 114: 487–493.
5. Hartick, J. W., Tacke, M. T., Fruchtel, G., P., H. E., and Janicka, J., Interactions of turbulence and radiation in confined diffusion flames, Proc. Combust. Institute 1996, 26: 75–82.
6. Mazumder, S. and Modest, M. F., A PDF approach to modeling turbulence-radiation interactions in nonluminous flames, Intern. J. Heat and Mass Trans. 1998, 42: 971–991.
7. Li, G. and Modest, M. F., Application of composition PDF methods in the investigation of turbulence-radiation interactions, J. Quant. Spectr. and Radiat. Trans. 2002, 73: 461–472.
8. Coelho, P. J., Teerling, O. J., and Roekaerts, D., Spectral radiative effects and turbulence/radiation interaction in a nonluminous turbulent jet diffustion flame, Combust. and Flame 2003, 133: 75–91.
9. Zheng, Y., Sivathanu, Y. R., and Gore, J. P., Measurements and stochastic time and space series simulations of spectral radiation in a turbulent non-premxied flame, Proc. Combust. Institute 2003, 29: 1957–1963.
10. Zimberg, M. J., Frankel, S. H., Gore, J. P., and Sivathanu, Y. R., A study of coupled turbulent mixing, soot chemistry, and radiation effects using the linear eddy model, Combust. and Flame 1998, 113: 454–469.
11. Bai, X. S., Balthasar, M., Mauss, F., and Fuchs, L., Detailed soot modeling in turbulent jet diffusion flames, Proc. Combust. Institute 1998, 17: 1623–1630.
12. Pitsch, H., Riesmeier, E., and Peters, N., Unsteady flamelet modeling of soot formation in turbulent diffustion flames, Combust. Sci. and Tech. 2000, 158: 389–406.
13. Barlow, R. S., website, http://www.ca.sandia.gov/TNF/, accessed on January 1, 2004.
14. Zhu, X. L., Gore, J. P., Karpetis, A. N., and Barlow, R. S., The effect of self-absorption of radiation on an opposed flow partially premixed flame, Combust. Flame 2002, 129: 342–345.
15. Mazumder, S. and Modest, M. F., Application of the full-spectrum correlated-k distribution approach to modeling nongray radiation in combustion gases, Combust. Flame 2002, 129: 416–438.
16. Kim, O. J., Gore, J. P., Viskanta, R., and Zhu, X. L., Prediction of self-absorption in opposed flow diffustion and partially premixed flames using a weighted sum of gray gases model (WSGGM)-based spectral model, Numerical Heat Transfer Part A-Applications 2003, 44(4): 335–353.
17. Ji, J., Sivathanu, Y. R., and Gore, J. P., Thermal radiation properties of turbulent lean premixed methane air flames, Proc. Combust. Institute 2000, 28: 391–398.
18. Zheng, Y., Barlow, R. S., and Gore, J. P., Measurements and calculations of spectral radiation intensities for turbulent non-premixed and partially premixed flames, Trans. of the ASME 2003, 125: 678–686.
19. Wang, L., Haworth, D. C., Turns, S. R., and Modest, M. F., Interactions among soot, thermal radiation, and NO_x emissions in oxgyen-enriched turbulent nonpremixed flames: a CFD modeling

study, Proc. Combust. Institute 2004:, submitted.
20. Cleaver, R. P., Cumber, P. S., and Fairweather, M., Predictions of free jet fires from high pressure sonic releases, Combust. Flame 2003, 132: 463–474.
21. Modest, M. F. and Zhang, H., The full-spectrum correlated-k distribution for thermal radiation from molecular gas-particulate mixtrues, Trans. ASME 2002, 124: 30–38.
22. Riazzi, R. and Modest, M., Assembly of Full-Spectrum k-Distribution from a Narrow-Band Database; Effects of Mixing Gases, Gases and Nongray Absorbing Particles, and Mixture with Nongray Scatters in Nongray Enclosures, J. Quant. Spectrosc. Raiat. Transf. 2004, in print.
23. Wang, L., Endrud, N. E., Turns, S. R., D'Agostini, M. D., and Slavejkov, A. G., A study of the influence of oxygen index on soot, radiation, and emission characteristics of turbulent jet flames, Combust. Sci. and Tech. 2002, 174(8): 45–72.
24. Baukal, C. E., *Oxygen-Enhanced Combustion*, CRC Press, Boca Raton 1998.
25. Turns, S. R., *An Introduction to Combustion: Concepts and Applications*, McGraw-Hill, New York 2nd edn. 2000.
26. Zhang, Y. Z. and Haworth, D. C., A general mass consistency algorithm for hybrid particle/finite-volume PDF methods, J. Comput. Phys. 2004, in print.
27. Appel, J., Bockhorn, H., and Frenklach, M., Kinetic modeling of soot formation with detailed chemistry and physics: laminar premixed flames of C_2 hydorcarbons, Combust. Flame 2000, 121: 122–136.
28. Smith, G. P., Golden, D. M., M., F., Moriarty, N. W., Eiteneer, B., Goldenberg, M., Bowman, C. T., Hanson, R. K., Song, S., Gardiner Jr., W. C., Lissianski, V. V., and Qin, Z., website, http://www.me.berkeley.edu/gri_mech/, accessed on January 1, 2004.
29. Wang, L., *Detailed chemistry, soot, and radiation calculations in turbulent reacting flows*, PhD thesis The Pennsylvania State University 2004.
30. Kee, R. J., Rupley, F. M., and Miller, J. A., Chemkin-II: a Fortran chemical kinetics package for the analysis of gas-phase chemical kinetics, Technical Report Report SAND89-8009 Sandia National Laboratories 1989.
31. Pope, S. B., Computationally efficient implementation of combustion chemistry using in situ adaptive tabulation, Combust. Theory & Modelling 1997, 1(1): 41–63.
32. Kong, S. C., Marriott, C. D., and Reitz, R. D., Modeling and experiments of HCCI engine combustion using detailed chemical kinetics with multidimensional CFD, SAE Paper 2001, 2001-01-1026.
33. Wang, H. and Frenklach, M., A detailed kinetic modeling study of aromatics formation in laminar premixed acetylene and ethylene flames, Combust. and Flame 1997, 110: 173–221.
34. Frenklach, M., Method of moments with interpolative closure, Chem. Engineering Sci. 2002, 57: 2229–2239.
35. Modest, M. F., Narrow-band and full spectrum k distribution for radiative heat transfer — correlated-k vs. scaling approximation, J. Quant. Spectrosc. Raiat. Transf. 2003, 76: 69–83.
36. Zhang, H. and Modest, F. M., Scalable multi-group full-spectrum correlated-k distributions for radiative transfer calculations, ASME J. Heat Trans. 2003, 125(3): 453–461.
37. Wang, A. and Modest, M. F., High-accuracy, compact database of narrow-band k-distribution for water vapor and carbon dioxide, J. Quant. Spectr. and Radiat. Trans. 2004, submitted.
38. Chang, H. and Charalampopoulos, T. T., Determination of the wavelength dependence of refractive indices of flame soot, Proc. of the Royal Society (London), Ser. A 1990, 430: 577–591.